ISCORMA-3, Cleveland, Ohio, 19-23 September 2005

DYNAMIC ANALYSIS OF A TURBOCHARGER IN FLOATING BUSHING BEARINGS

Edgar J. Gunter
RODYN VIBRATION ANALYSIS, INC.
1932 Arlington Blvd., Suite 223
Charlottesville, VA 22903
DrGunter@aol.com

Wen Jeng Chen
Eigen Technology, Inc.
P.O. Box 2224
Davidson, NC 28036
WJChen@dyrobes.com

ABSTRACT

This paper presents the linear and nonlinear dynamical behavior of a typical turbocharger in floating bush bearings. In this paper, the linearized stability of the system was computed for various bushing inner and outer clearance ratios. The turbocharger has two principal modes in which it can exhibit whirl instability. The first is a conical mode which is essentially a rigid body mode. The second mode is an in-phase whirling mode in which over 50% of the system strain energy is associated with shaft bending. These whirling modes may be only 1/6 and 1/4 of running speed. Experimental data indicates that either one or both of these modes may exist simultaneously. Although the turbocharger exhibits self excited bearing instability at very low onset speeds, the turbocharger is able to operate with controlled limit cycle motion at speeds of 100,000 RPM and higher due to the nonlinear action of the fluid film floating bush bearings. In order to examine limit cycle motion, the system finite element dynamical equations of motion were numerically integrated forward in time. Included also in the analysis are the effects of rotor unbalance and destabilizing Alford type forces acting at the compressor and turbine wheels. These effects can strongly influence the limit cycle orbits and the bearing forces transmitted. The rotor could be made to whirl in either the first conical mode or the second in-phase mode by changes in the compressor or turbine bushing bearing clearances.

A third bending critical speed was evaluated for unbalance response. This third mode may occur at peak speeds and may limit the maximum operating speed due to the high compressor bearing forces encountered and subsequent shaft bending.

Keywords: turbocharger, stability, limit cycle motion, rotor whirling, time transient rotor dynamics

INTRODUCTION

The dynamical analysis of a turbocharger represents a number of challenging problems. The typical turbocharger is often referred to as a double overhung rotor. That is, the turbine and compressor wheels are outboard of the bearings. These turbochargers can operate in a speed range exceeding 100,000 RPM. The type of bearing and damper design for a turbocharger is dictated by its size and performance capabilities. For example, a large turbocharger for a diesel locomotive may have a 3 lobe or offset bearing supported in a centered squeeze-film damper. These elaborate bearing designs are not possible in the smaller turbochargers that are used in automotive applications due to size and cost considerations. A standard type of bearing employed with automotive turbochargers is the floating bush bearing.

Turbocharger Design With Floating Bushing Bearings

Fig. 1 represents a schematic drawing of a typical turbocharger as presented by Li (1982). The figure of Li has been modified to show the floating bushing bearings.

The turbocharger consists a the steel turbine wheel as shown on the right and an aluminum compressor wheel as shown in Fig. 2. The turbocharger is supported by two floating bush bearings. The floating bush bearing is free to rotate. The rate of the bushing rotation is a fraction of shaft speed. The bearing inner clearance is normally smaller than the outer bushing clearance. The turbine wheel is integral with the shaft. The aluminum compressor wheel is machined for line to line contact and bolted on to the shaft.

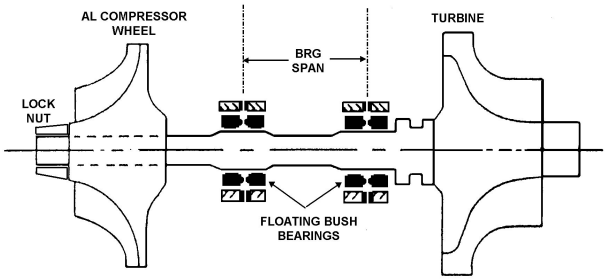

Fig. 1 Turbocharger in Floating Bush Bearings
(Li 1982)

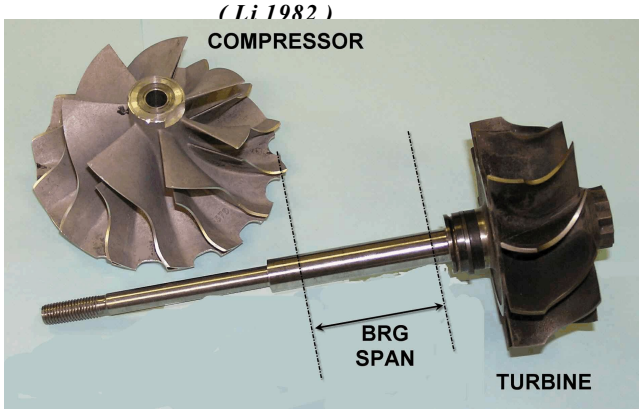

Fig. 2 Dissembled Turbocharger Showing Compressor Wheel And Bearing Span

Fig. 3 Turbocharger Floating Bush Bearings

The typical type of bearing used in these lightweight, low-cost turbochargers is the floating bush bearings, as shown in Fig. 3. The theory of the floating bush bearing was presented as early as 1949 by Shaw and Macks in their classical lubrication textbook on *Analysis and Lubrication of Bearings*. The original design concept for the floating bush bearing was to reduce friction losses. The ring is free to rotate. The design of the floating bush is such that the inner clearance is smaller than the outer clearance. The ring then rotates at a fraction of shaft speed. The ring speed is determined by the friction torque balance between the inner and outer films. By expressing the

Reynolds equation governing the pressure profile in rotating coordinates, Shaw and Macks explain the mechanism by which the floating bush bearing generates a pressure profile as a combination of ring rotation, ring precession rate, and radial squeeze film motion..

The pressure profile is generated by the rotational speed of the ring, its precessional rate, and its local eccentricity velocity. For circular orbiting about the origin, this last term may be ignored. The modeling of the floating bush bearing can become quite extensive, and the analysis is assisted by experimental data. One of the major problems in the analysis of the floating bush is the assumption of the ring speed. Theoretically, one could have a ring speed approaching one-half of shaft rotation, but this value never occurs in practice. Quite often, what is observed is a uniform increase in ring speed as a percentage of shaft speed until, at given speed, the ring speed is constant. In this analysis, ring speed was assumed to be 20% of shaft speed although Li measured values as low as 11%. Detailed analysis of the ring, including thermal effects, show that the inner temperature can be substantially higher than the outer film temperature. The high inner temperature reduces the viscosity and causes a limit of the speed of rotation of the ring.

The floating bush ring is commonly employed because it is inexpensive to produce. However, with a fixed journal bearing, the stability is extremely poor as compared to a lobed or tilting-pad bearing. The rotation of the outer surface of the floating bush bearing acts as an uncentered squeeze-film damper. The analysis is difficult because, even with the assumption of ring speed, the system is nonlinear. One can, however, perform a linearized analysis to determine the stiffness and damping coefficients of both the inner and outer clearances. The linearized stability analysis shows that the system is unstable at speeds of 100,000 RPM. In fact, the onset speed can be extremely low. In addition to being unstable, the instability can be exhibited in either the first mode, which has a conical mode shape, or in the second mode, which involves shaft bending. The earlier analysis of Li (1982) did not have enough degrees of freedom to show the second unstable mode or the rotor third bending critical speed.

Experimental Turbocharger Whirl Motion

Fig. 4 represents a typical turbocharger as shown by Holmes (2004). The turbocharger exhibits whirl instability at a very low speed. This low frequency whirl is of a conical nature with the turbine and compressor wheels moving out of phase. This subsynchronous motion continues over a large speed range. A second whirl component is seen at speeds above 40,000 RPM. This second mode is associated with the in-phase turbocharger 2nd forward resonance frequency.

Of particular interest is the observation of restabilization of the second whirling mode at speeds around 55,000 RPM. This restabilization may be due to the slight increase in bearing loading due to the possible presence of the turbocharger 3rd mode. At speeds above 70,000 RPM, the 2nd whirling mode appears to dominate. As the speed is increased further, the limit cycle motion of the second mode appears to cause the whirling in the conical mode to vanish. This may be caused by the increase in bearing loading due to the high limit cycle motion above 70,000 RPM.

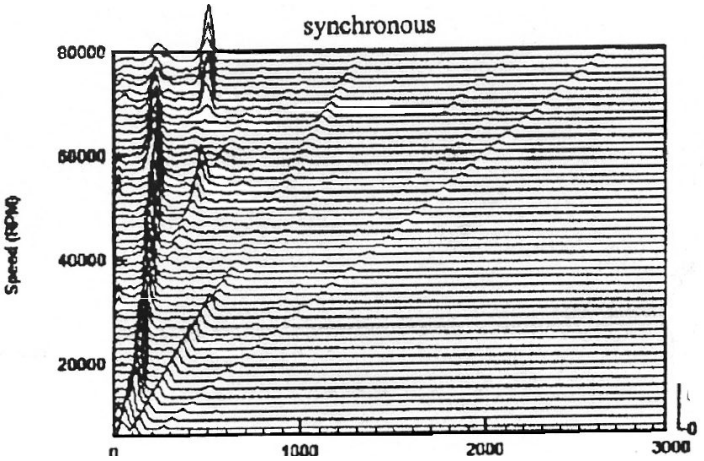

Fig. 4 Typical Turbocharger Waterfall Diagram (Holmes 2004)

Although the floating bush bearing may be unstable in the linear sense, when a nonlinear time transient analysis is performed, then limit cycle whirl motion is observed. This limit cycle whirl motion is a bounded motion, and the turbocharger may operate for an extended time with bounded limit cycle whirl motion. There is the added paradox that rotating unbalance load may actually result in a lower limit cycle whirl motion than a well-balanced rotor. In this paper, a typical turbocharger in floating bush bearings is analyzed for nonlinear transient motion with various clearance conditions and unbalances. In addition to the problems of limit cycle whirl motion, which may be quite large under certain circumstances, there is an additional problem that can be encountered with turbochargers. As designs are attempted to run over 100,000 RPM, then certain turbochargers are encountering the third flexible critical speed. This mode is very difficult to balance out and may have a high amplification factor leading to rubbing and bearing distress.

Fig. 5 represents an interesting turbocharger design with an inducer stage in front of the compressor. This type of turbocharger design presents unique problems in having a third bending critical speed in the operating speed range. The existence of the 3rd bending critical speed may often limit the upper operating speed of a turbocharger.

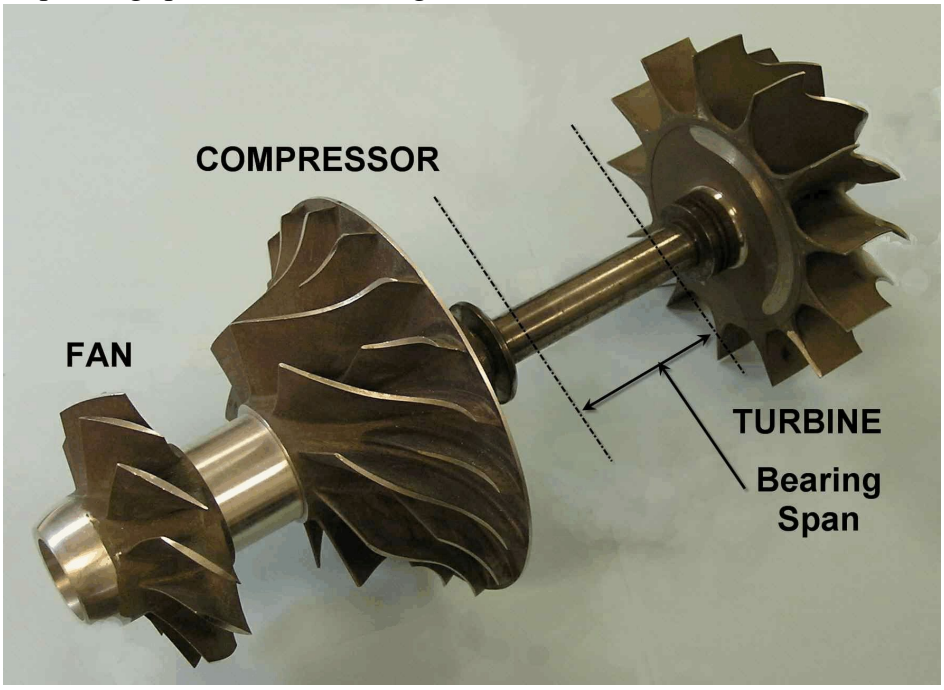

Fig. 5 Turbocharger With Axial Fan Stage

TURBOCHARGER DYNAMICAL ANALYSIS

Critical Speed Analysis

Although the dynamics of the turbocharger in floating bush bearings is highly nonlinear, it is still useful to examine the simple critical speeds and mode shapes of the turbocharger. In addition to the synchronous critical speeds, from the experimental data, one can observe the whirl frequencies from the data. It is then possible to compute the effective bearing impedance from the experimental data. From the observation of the mode shape and energy distribution of the third mode, it is seen that this mode has no potential energy in the turbine bearing and also very little energy in the compressor bearing. This makes it difficult for the turbocharger to operate through the third critical speed due to high synchronous vibrations. This appears to be the situation that was encountered with the turbocharger as shown in Fig. 5. The maximum speed is limited by the low third critical speed. The third critical speed should be above the maximum operating speed.

Modeling Assumptions

Fig. 6 represents the turbocharger model for critical speed analysis. There are several major assumptions involved in the basic modeling of the turbocharger. The first assumption concerns the attachment of the aluminum compressor wheel onto the steel shaft. At speeds of 100,000 RPM and higher, the aluminum compressor does not add stiffening to the shaft. Therefore, as seen in this model, the stiffness of the system is provided by the steel shaft alone. One of the methods of turbocharger analysis is by the use of free-free modes. These free-free modes are compared to the experimental modes of the turbocharger from a simple rap test. This can be very deceptive since the frictional interface of the compressor wheel and attachment nut makes the compressor appear to be an integral unit. Extensive finite element analysis studies of the compressor wheel and shaft has shown that this is not the case at high speed. The compressor wheel is assembled with line-to-line contact. At speed, the compressor provides little shaft stiffening effects due to centrifugal growth.

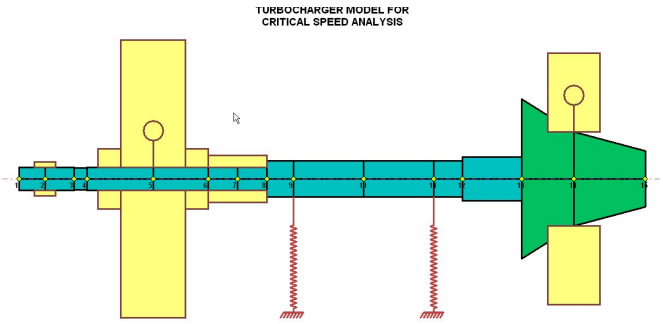

Fig. 6 Turbocharger Model For Critical Speed Analysis

A second major assumption concerns the effective polar moment of inertia of the compressor wheel which enters into the gyroscopic calculations. From an examination of experimental data and three dimensional finite element compressor wheel analysis with centrifugal forces, the polar moment of inertia of the compressor wheel may need to be reduced by 20% to produce accurate dynamical moment calculations. This reduction of gyroscopic inertia moment occurs in large overhung utility fan wheels and in LP aircraft overhung turbine stages. This is due to the flexibility of the compressor wheel and the lack of a solid connection between the aluminum wheel and the steel turbocharger shaft at high speeds. These assumptions lead to a significant reduction in the third critical speed.

Critical Speeds and Strain Energy Distribution

The undamped natural frequencies calculations were generated to provide insight into the fundamental turbocharger mode shapes and also evaluate the relative potential energy distribution of the shaft and bearings for a given mode. The values of the nominal bearing stiffness used are based on observed critical speeds and whirl frequencies observed at running speed. This analysis was actually performed after an extensive amount of nonlinear studies were conducted.

Nominal Turbocharger Critical Speeds and Potential Energy Distribution

Fig. 7 represents the first critical speed of the turbocharger for nominal assumed value of total effective bearing stiffness of 50,000 Lb/In.

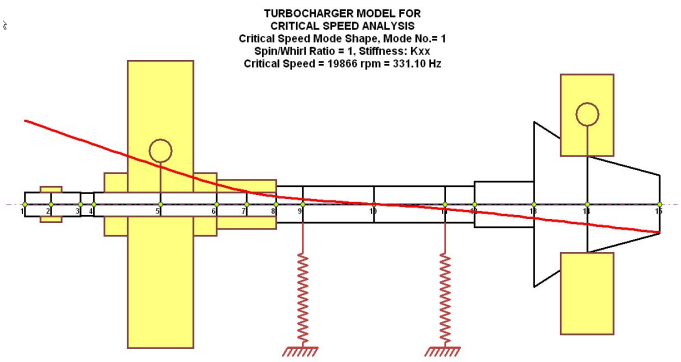

Fig. 7 1st Critical Speed At 19,000 RPM

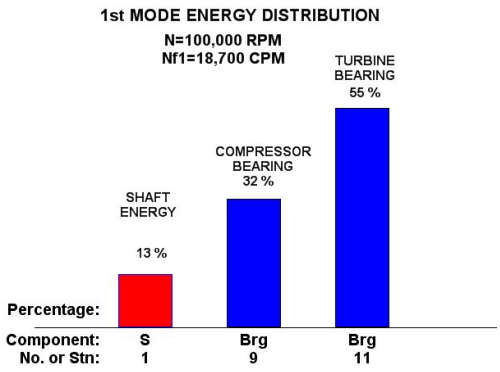

Fig. 8 Potential Energy Distribution For 1st Forward Mode At 100,000 RPM

The first mode is essentially a rigid body conical mode in which the turbine and compressor wheels are out of phase. Fig. 8 represents the relative potential shaft and bearing energy distributions. For the first mode, the potential energy is greatest in the turbine bearing. This is due to the heavier weight of the turbine wheel. Thus the turbine bearing will have a greater control over the first critical speed and the conical whirl instability encountered at higher speeds.

Figures 9 and 10 represents the 2nd mode and the corresponding energy distributions. In this mode the shaft bending energy has increased to 64% and the turbine potential bearing has reduced to 17%. The compressor bearing energy is 19%. The turbine and compressor wheels are in phase.

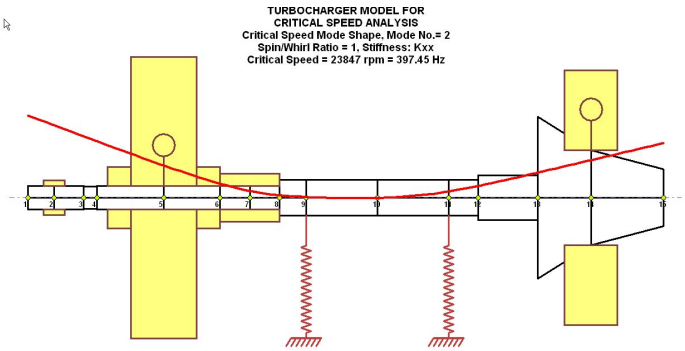

Fig. 9 2nd Critical Speed At 23,847 RPM

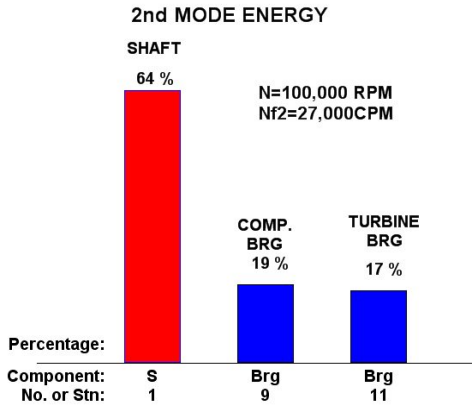

Fig. 10 Potential Energy Distribution For 2nd Forward Mode At 100,000 RPM

Fig. 11 represents the third turbocharger critical speed at 102,895 RPM. This mode is shown to be in the operating speed range of the turbocharger. When the compressor wheel no longer provides shaft stiffening due to wheel centrifugal growth, then the long overhang at the compressor section may cause a critical speed to occur within the operating speed range. This third shaft bending critical speed is normally not predicted by modal methods due to the assumption of the mode shapes. In Fig. 13, it is seen that the turbine bearing is a node point and hence provides no damping to control the third critical speed. The compressor bearing has only 17% potential energy.

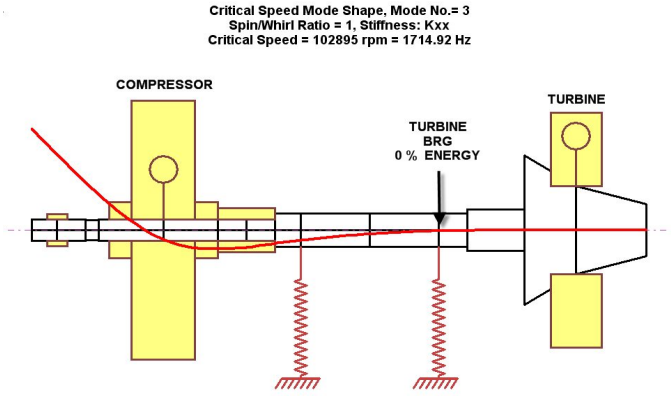

Fig. 11 3rd Critical Speed At 103,000 RPM

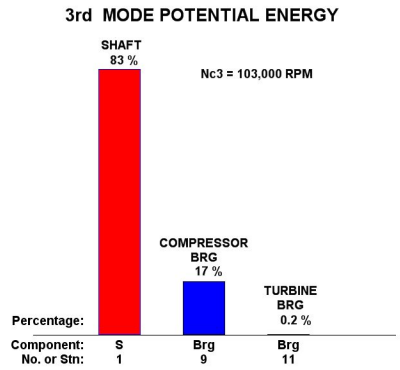

Fig. 12 Potential Energy Distribution For 3rd Critical Speed At 103,000 RPM

In Fig. 11 for the 3rd critical speed, over 83% of the shaft strain energy is associated with bending under the compressor wheel. The 3rd turbocharger bending mode is very susceptible to unbalance excitation caused by compressor shaft bow or disk skew at 100,000 RPM which is design speed.

Turbocharger Damped Natural Frequencies (Complex Eigenvalues)

Fig. 13 represents the turbocharger model with the floating bushing bearings added. Two additional bearing stations have been added in order to assign values of aerodynamic cross coupling acting at the turbine and compressor stations. Fig. 14 represents the specification of the floating bushing characteristics such as clearances, film viscosities and ring spin speed ratio. The inner ring diametral clearance Cdi is 2 mils and the outer ring clearance Cdo is taken as 4 mils.

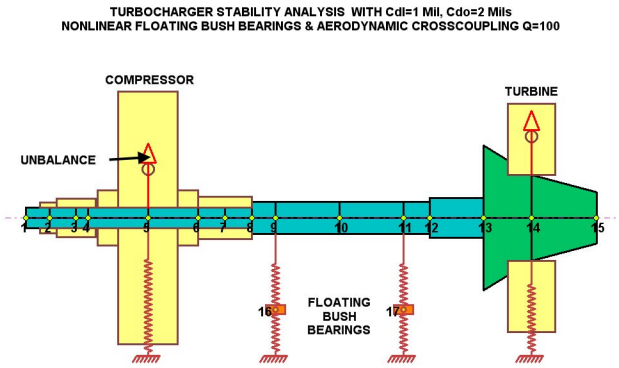

Fig. 13 Turbocharger Model With Floating Bush Bearings And Aerodynamic Cross Coupling

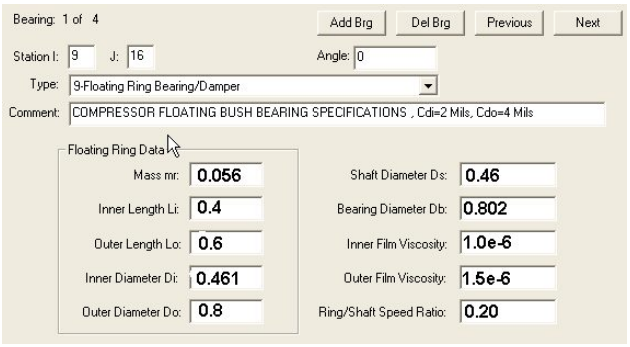

Fig. 14 Characteristics of Floating Bush Bearing

Fig. 15 shows the first forward whirl mode at 100,000 RPM with a small amount of aerodynamic cross-coupling of 100 Lb/In acting at both the compressor and turbine wheels. The whirl mode is essentially a rigid body conical mode with the turbine end bearing having the predominant effect. Fig. 16 shows the second forward mode at 100,000 RPM. In this case, there is substantial shaft bending with the largest motion at the compressor end. This mode is only marginally stable as the log decrement is only 0.022. This mode may also become unstable.

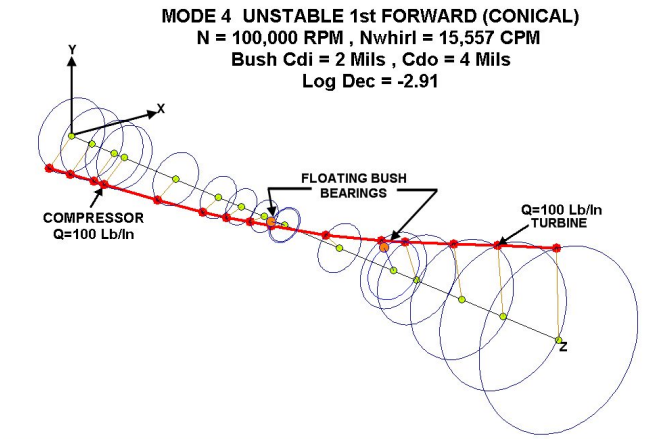

Fig. 15 Unstable Forward Conical Mode At 100,000 RPM Nf1 = 15,557 CPM, Log Dec = -2.9

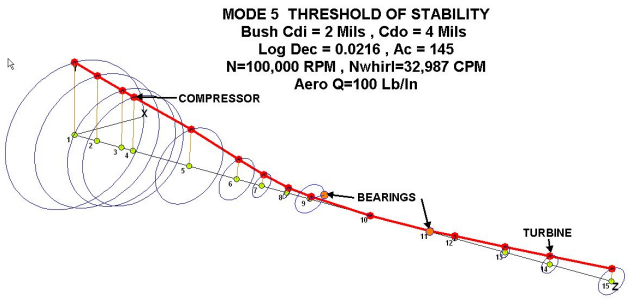

Fig. 16 Marginally Stable 2nd Forward Whirl Mode At 100,000 RPM, Nf2=32,987 CPM, Log Dec = 0.0216

For the first conical mode as shown in Fig. 15, the turbine bearing has the most influence. The stability in this mode is improved by a reduction of clearance in the turbine bearing. It is usually not practical to close the turbine bearing up too tightly as there are cases of the ring welding on to the shaft. For the in-phase second whirl mode as shown in Fig. 16, the compressor end bearing has more influence then the turbine end bearing. An increase of inner ring clearance on the compressor bearing may induce the second whirling mode.

Turbocharger Nonlinear Unbalance Response

Fig. 17 represents the nonlinear synchronous unbalance response of the turbocharger in the floating bush bearings. The motion of the shaft is assumed to be circular synchronous. The bearing radial and tangential forces increase with the bearing eccentricity orbit. A large response is seen at the compressor nut at a speed of 123,000 RPM. This value is slightly higher than the computed undamped third critical speed as shown in Fig. 11. The difference in the higher forced response speed is due to the nonlinear bearing forces which may vary with speed and bearing loading.

Fig. 18 shows the 3 dimensional shaft mode shape with the unbalance of 0.005 oz-in at the compressor and turbine wheels at a 90 deg phase separation. At the speed of 123,000 RPM, these values of unbalance generate rotating loads of 134 lb. The transmitted load at the compressor bearing is 160 lb and only 62 lb at the turbine bearing. Note that a proximity probe placed between the bearings will not detect the presence of the third critical speed.

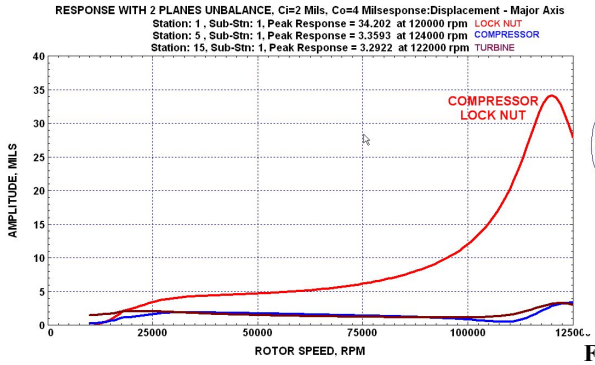

Fig. 17 Turbo Synchronous Unbalance Response

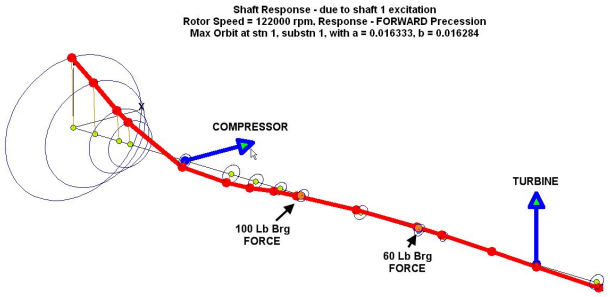

Fig. 18 Shaft Unbalance Mode Shape At 122,800 RPM With Compressor and Turbine Unbalance At 90 Deg

Turbocharger Time Transient Motion

The turbocharger mounted in floating bush bearings is unstable with self excited whirl motion starting at a relatively low speed. The turbocharger is able to operate at speed without immediate failure due to the nonlinear bearing forces. The rotor is able to operate at speed in limit cycle motion. In order to understand the nature of the limit cycle motion and the bearing forces transmitted, it is necessary to perform a time transient analysis in which the rotor equations of motion are numerically integrated with respect to time. Fig. 19 shows the integration options used for the transient.

Initial Time Transient Motion With Normal And Seized Bushing Bearings.

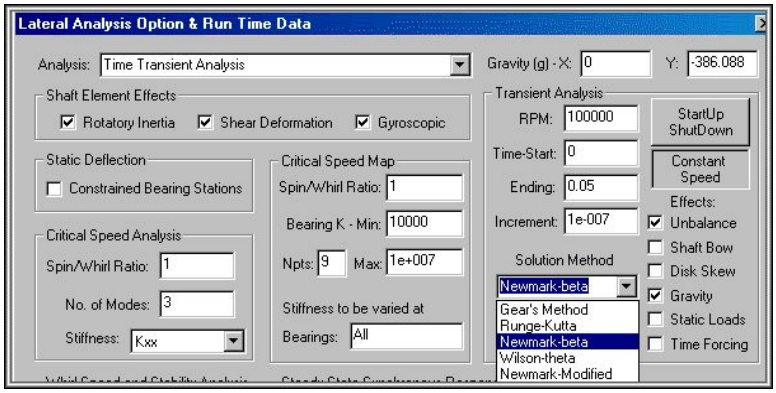

Fig. 19 Time Transient Analysis Options For Integration Method, Time Steps and Rotor Forcing Functions

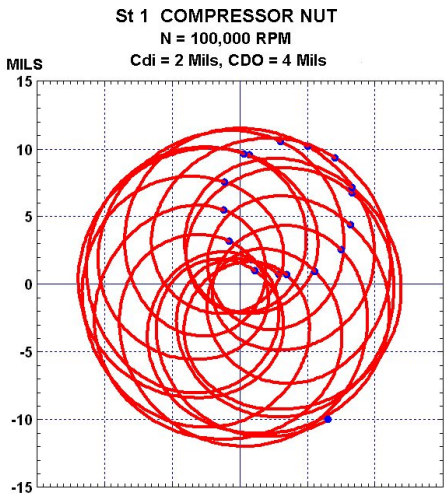

Fig. 20 Limit Cycle Whirl Motion At St 1 After Initial 20 Cycles of Shaft Motion

Fig. 20 shows the compressor whirl at station 1 in limit cycle motion with p-p amp of 24 mils.

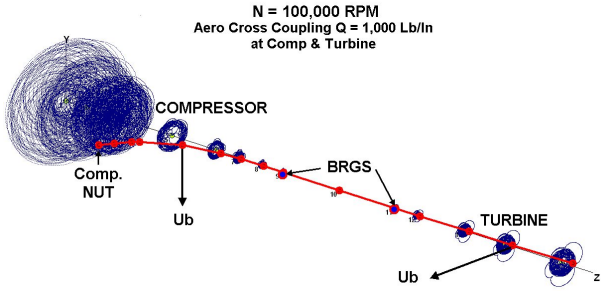

Fig. 21 Initial Transient Motion With 2 Planes Ub N=100,000 RPM, Cdi = 2 Mils, Cd0 = 4Mils

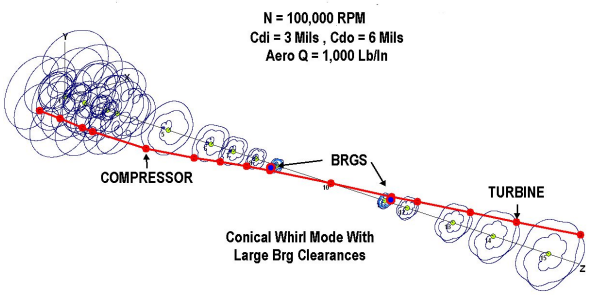

Fig. 22 Initial Transient With Enlarged Bushing Clearances, Cdi = 3 Mils, Cd0 = 6Mils

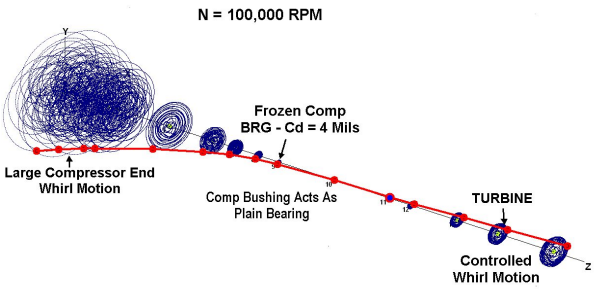

Fig. 23 Initial Transient Motion With Locked Compressor Bushing- Cd = 4Mils

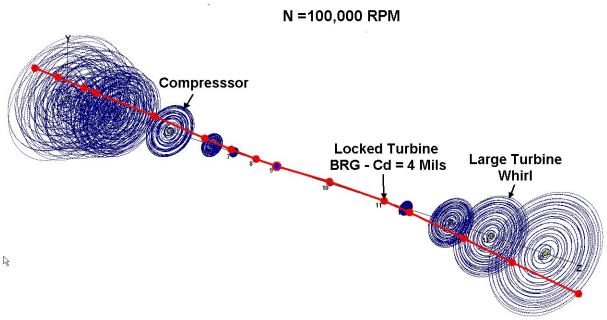

Fig 24 Initial Transient Motion With Locked Turbine Bushing- Cd = 4 Mils

Fig. 21 represents the initial transient motion with close clearance bushings. From Fig. 20 it is seen that limit cycle motion is achieved after 20 cycles of shaft motion. If the inner clearance Cdi is opened up from 2 to 3 mils and the outer clearance Cdo from 4 to 6 mils, then the whirl mode is a pronounced conical whirl as shown in Fig. 22.

Under certain conditions, the compressor or turbine bushing may become welded to the shaft. The locked bearing then acts as a plain bearing with the corresponding outer bushing clearance now being the effective bearing clearance as shown in Figs. 23 and 24. This large whirl motion may lead to damage of either the compressor or turbine.

DISCUSSION AND CONCLUSIONS

High speed turbochargers in floating bushing are inherently unstable from a linear standpoint. However the rotor is able to operate with controlled limit cycle motion due to the presence of nonlinear bearing forces. The bushing inner bearing clearance is normally kept at a very close clearance. If the bearing clearances are increased, then the whirl motion will increase and the rotor will whirl predominately in the conical mode.

Due to the tight bearing clearances used, one may encounter a condition in which either the compressor or turbine bearing becomes welded to the shaft. When this occurs, then the bushing acts as a plain bearing and the larger outer bushing clearance becomes the effect plain bearing clearance. Under these circumstances, the bearing is highly unstable and turbocharger life is greatly reduced. Turbo or bearing damage and wear may occur if the turbo operates near the third critical speed. High compressor bearing forces and amplitudes may occur at the third critical speed. It is recommended that superior synthetic (designer) lubricants be used in high speed turbos.

REFERENCES

1 Alford, J., "Protecting Turbomachinery from Self-Excited Rotor Whirl", ASME Journal of Engineering for Power, pp. 333-337, 1965.

2. Barrett, L. E., and E. J. Gunter, *Steady-State and Transient Analysis of a Squeeze Film Damper Bearing for Rotor Stability*, NASA CR-2548, 1975.

3. Chen, W. J., and E. J. Gunter, "*Introduction to Dynamics of Rotor-Bearing Systems*" TRAFFORD Publishing, Victoria, BC, Canada, 2005.

4. Dworski, J., "High-Speed Rotor Suspension Formed by Fully Floating Hydrodynamic Radial and Thrust Bearings, "ASME Journal of Engineering for Power, Vol. 86, pp. 149-160, 1964.

5. Gunter, E. J., and W. J. Chen, "*DyRoBeS Dynamics of Rotor-Bearing Systems, Windows Version 8, Users' Manual*, RODYN Vibration Analysis, Inc., Charlottesville, VA., 2003.

6. Hill, H. C., "Slipper Bearings and Vibration Control in Small Gas Turbines," ASME, Vol 80, pp. 1756-1764, 1958.

7. Holmes, R., "Turbocharger Vibrations - Case Study," Institute of Mechanical Engineering Conference on Turbochargers and Turbocharging, pp. 91-100, 2002.

8. Holmes, R., "Vibrations of An Automotive Turbocharger - A Case Study," C623, Institute of Mechanical Engineering, pp. 445-450, 2004.

9. Kettleborough, C. F., "Frictional Experiments on Lightly-Loaded Fully Floating Journal Bearings," Australian Journal of Applied Science, pp. 211-220, 1955.

10. Kirk, R. G. and E. J. Gunter, "Nonlinear Transient Analysis of Multi-Mass Flexible Rotors - Theory and Applications," NASA CR-2300, NASA, Washington, D.C, 1973.

11. Li, C. H., "On the Steady State and Dynamic Performance Characteristics of Floating Ring Bearings," Trans. ASME Journal of Lubrication Technology, Vol 103, pp. 389-397, 1981.

12. Li, C. H., "Dynamics of Rotor Bearing System Supported by Floating Ring Bearings," Trans. ASME Journal of Lubrication Technology, Vol 104, pp. 469-477, 1982.

13. Nakagawa, E., and H. Aoki, 1973, "Unbalance Vibration of a Rotor-Bearing System Supported by Floating-Ring Journal Bearings," Bull. ASME, Vol 16, 93, pp. 503-512.

14. Nikolajsen, J. L., "The Effect of Variable Viscosity on the Stability of Plain Journal Bearings and Floating-Ring Journal Bearings," ASME Paper 73-Lub-H, 1973.

15. Rohde, S. M. and H. A. Ezzat, "Analysis of Dynamically Loaded Floating-Ring Bearings for Automotive Application," Trans. ASME Journal of Lubrication Technology, Vol. 102, pp. 271-277, 1980.

16. Shaw, M. C. and T. J. Nussdorfer, "An Analysis of the Full-Floating Journal Bearing," NACA Report No. 866, 1947.

17. Shaw, M. C. and F. Mack, *Analysis And Lubrication Of Bearings*, McGraw-Hill, New York, 1949.

18. Tanaka, M. and Y. Hori, "Stability Characteristics of Floating Bush Bearings," ASME Journal of Lubrication Technology, Vol 94, pp. 248-259, 1972.

19. Tartara, A., "An Experimental Study of the Stabilizing Effect of Floating-Bush Journal Bearings," Bull. ASME, Vol 13, 61, pp. 858-863 , 1972.

20. Trippett, R. J. and D. F. Li, "High Speed Floating-Ring Bearing Test and Analysis," ASME Trans., Vol 27, pp. 73-81, 1983.